

Northumbria Research Link

Citation: Braddock, Scott, Hall, Brenda L., Johnson, Joanne S., Balco, Greg, Spoth, Meghan, Whitehouse, Pippa L., Campbell, Seth, Goehring, Brent M., Rood, Dylan H. and Woodward, John (2022) Relative sea-level data preclude major late Holocene ice-mass change in Pine Island Bay. *Nature Geoscience*, 15 (7). pp. 568-572. ISSN 1752-0894

Published by: Nature Publishing

URL: <https://doi.org/10.1038/s41561-022-00961-y> <<https://doi.org/10.1038/s41561-022-00961-y>>

This version was downloaded from Northumbria Research Link:
<https://nrl.northumbria.ac.uk/id/eprint/49249/>

Northumbria University has developed Northumbria Research Link (NRL) to enable users to access the University's research output. Copyright © and moral rights for items on NRL are retained by the individual author(s) and/or other copyright owners. Single copies of full items can be reproduced, displayed or performed, and given to third parties in any format or medium for personal research or study, educational, or not-for-profit purposes without prior permission or charge, provided the authors, title and full bibliographic details are given, as well as a hyperlink and/or URL to the original metadata page. The content must not be changed in any way. Full items must not be sold commercially in any format or medium without formal permission of the copyright holder. The full policy is available online: <http://nrl.northumbria.ac.uk/policies.html>

This document may differ from the final, published version of the research and has been made available online in accordance with publisher policies. To read and/or cite from the published version of the research, please visit the publisher's website (a subscription may be required.)

1 **Relative sea-level data preclude major late Holocene**
2 **ice-mass change in Pine Island Bay**

3 Scott Braddock¹, Brenda L. Hall^{1*}, Joanne S. Johnson², Greg Balco³, Meghan Spoth¹,
4 Pippa L. Whitehouse⁴, Seth Campbell¹, Brent M. Goehring⁵, Dylan H. Rood⁶, John
5 Woodward⁷

6 ¹ School of Earth and Climate Sciences and the Climate Change Institute, University of
7 Maine, Orono, Maine, USA.

8 ² British Antarctic Survey, Cambridge, UK.

9 ³ Berkeley Geochronology Center, Berkeley, CA, USA

10 ⁴ Department of Geography, Durham University, Durham, UK

11 ⁵ School of Science and Engineering, Tulane University, New Orleans, USA

12 ⁶ Department of Earth Science and Engineering, Imperial College, London, UK

13 ⁷ Department of Geography and Environmental Sciences, Northumbria University,
14 Newcastle upon Tyne. UK

15 *Corresponding author : e-mail: brendah@maine.edu

16

17 **The rapidly retreating Thwaites and Pine Island glaciers together dominate**
18 **present-day ice loss from the West Antarctic Ice Sheet (WAIS) and are implicated**

19 **in runaway deglaciation scenarios. Knowledge of whether these glaciers were**
20 **substantially smaller in the mid-Holocene and subsequently recovered to their**
21 **present extents is important for assessing if current ice recession is irreversible.**
22 **Here, we reconstruct relative sea-level (RSL) change from radiocarbon-dated**
23 **raised beaches at sites immediately seaward of these glaciers, allowing us to**
24 **examine the response of the earth to loading and unloading of ice in the**
25 **Amundsen Sea region. We find that RSL fell steadily over the past 5.5 ka without**
26 **rate changes that would characterize large-scale ice re-expansion. Moreover,**
27 **current bedrock uplift rates are an order of magnitude greater than the rate of**
28 **long-term RSL fall, suggesting a change in regional crustal unloading and**
29 **implying that the present deglaciation may be unprecedented in the last ~5.5 ka.**
30 **While we cannot preclude minor grounding-line fluctuations, our data are**
31 **explained most easily by early Holocene deglaciation followed by relatively stable**
32 **ice positions until recent times and imply that Thwaites and Pine Island Glaciers**
33 **have not been substantially smaller than present during the last 5.5 ka.**

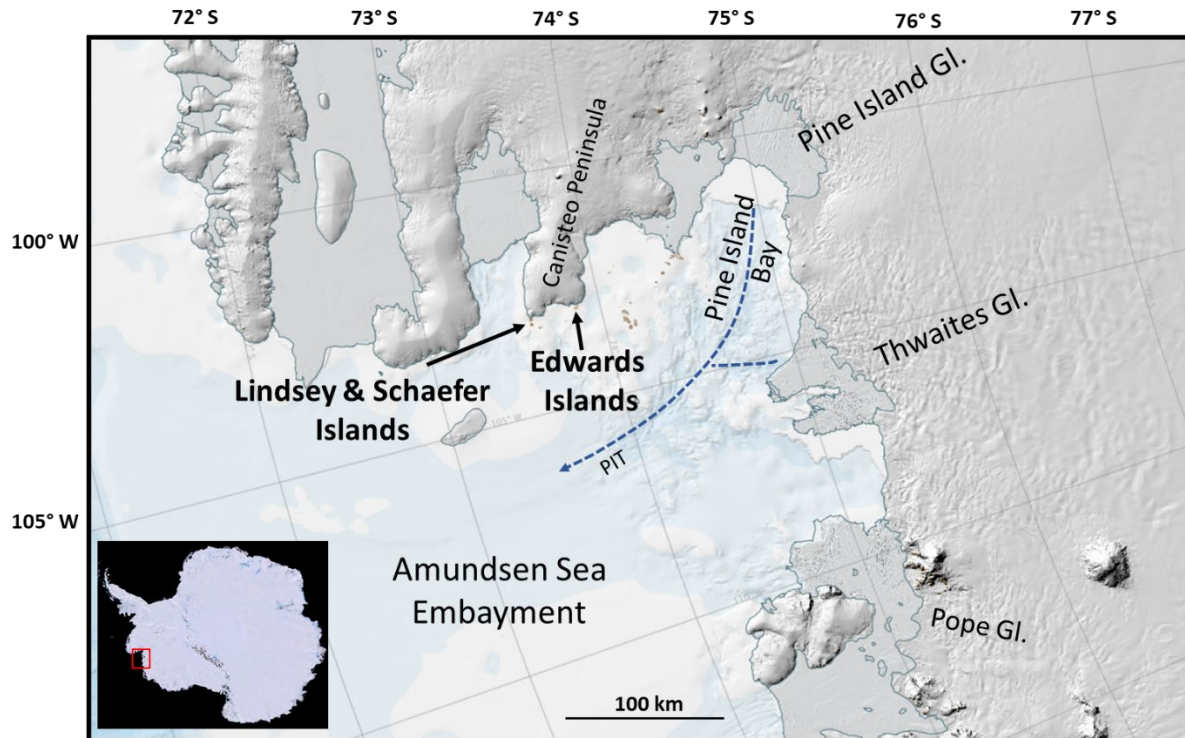
34

35 WAIS behavior under future global warming scenarios remains a great uncertainty in
36 sea-level projections¹. Over recent decades, the WAIS has retreated and thinned at
37 accelerating rates in the Amundsen Sea Embayment and is predicted to continue this
38 trend^{2,3}. Of concern is the ongoing mass loss of Thwaites and Pine Island Glaciers (Fig.
39 1), which together drain a large portion of the Amundsen Sea sector and reach deep
40 into the heart of the WAIS. These glaciers are susceptible to rapid retreat, because they
41 are being melted from beneath by warm Circumpolar Deep Water^{4,5}. Moreover,

42 Thwaites and Pine Island Glaciers rest below sea level on a retrograde slopes with no
43 known major topographic highs on which the glaciers could stabilize, and therefore they
44 may be susceptible to runaway retreat via marine ice-sheet instability^{6,7}. Such retreat is
45 likely to trigger extensive ice loss of the WAIS^{8,9}, contributing as much as 3.4 m to
46 global sea level over the next several centuries¹⁰.

47 Geologic evidence has provided insight into ice behavior in the Amundsen Sea sector.
48 Existing data show that Thwaites¹¹ and Pine Island¹² glaciers previously merged in Pine
49 Island Trough to form a paleo-ice stream, which extended to the continental shelf edge
50 at the Last Glacial Maximum^{13,14}. Marine radiocarbon and terrestrial exposure-age
51 dating show deglaciation of the outer embayment at 12-9 ka^{15,16}, with the grounding line
52 reaching close to its current position by the early Holocene^{14,15}. Cosmogenic exposure-
53 age studies on nunataks near Pope and Pine Island Glaciers indicate that ice in this
54 region thinned to current elevations by the mid-Holocene^{17,18} (Fig. 1).

55 However, the lack of evidence for ice behavior since the mid-Holocene allows two
56 plausible hypotheses: 1) Thwaites and Pine Island Glaciers reached their current
57 configuration in the mid-Holocene and have remained stable until very recently, or 2)
58 these glaciers continued to retreat to positions behind present-day margins until
59 subsequent readvance to near current limits in the late Holocene. The former would
60 suggest that the recent rapid ice loss from these glaciers is unprecedented over the last
61 5 ka and could evolve into runaway retreat^{7,8}, whereas the latter would imply that
62 current rapid ice recession could be reversible. Discriminating between these scenarios
63 is becoming increasingly urgent, as some have proposed irreversible retreat of Thwaites
64 Glacier may be underway^{19,20}.



65
 66 **Fig. 1. Map of Amundsen Sea Embayment, Antarctica, showing sites mentioned in**
 67 **the text.** Our study locations are shown in bold text. Textured gray represents the
 68 current ice sheet surface (from Reference Elevation Model of Antarctica (REMA)²¹).
 69 Shaded gray areas outlined in blue represent ice shelves. Dashed blue lines indicate
 70 former ice flow directions through Pine Island Trough (PIT). Bathymetry (blue and white
 71 shades) from GEBCO2019 global data set²². Map from the SCAR Antarctic Digital
 72 Database.

73

74 Records of RSL reflect the combined effect of global ocean volume change and local
 75 perturbations to the solid Earth and geoid due to glacial isostatic adjustment (GIA).
 76 Thus, determining the timing and pattern of Holocene RSL variation can provide
 77 information on local ice history since the Last Glacial Maximum, as well as on current
 78 and past rates of rebound directly related to ice-mass fluctuations (e.g. ^{23,24}). Today,
 79 rapid uplift is prevalent in the Amundsen Sea Embayment region, where current rates
 80 exceed 40 mm/yr in some locations²⁵. Holocene RSL data afford information on whether
 81 such rates are anomalous and can identify transgressions or periods of slowing RSL

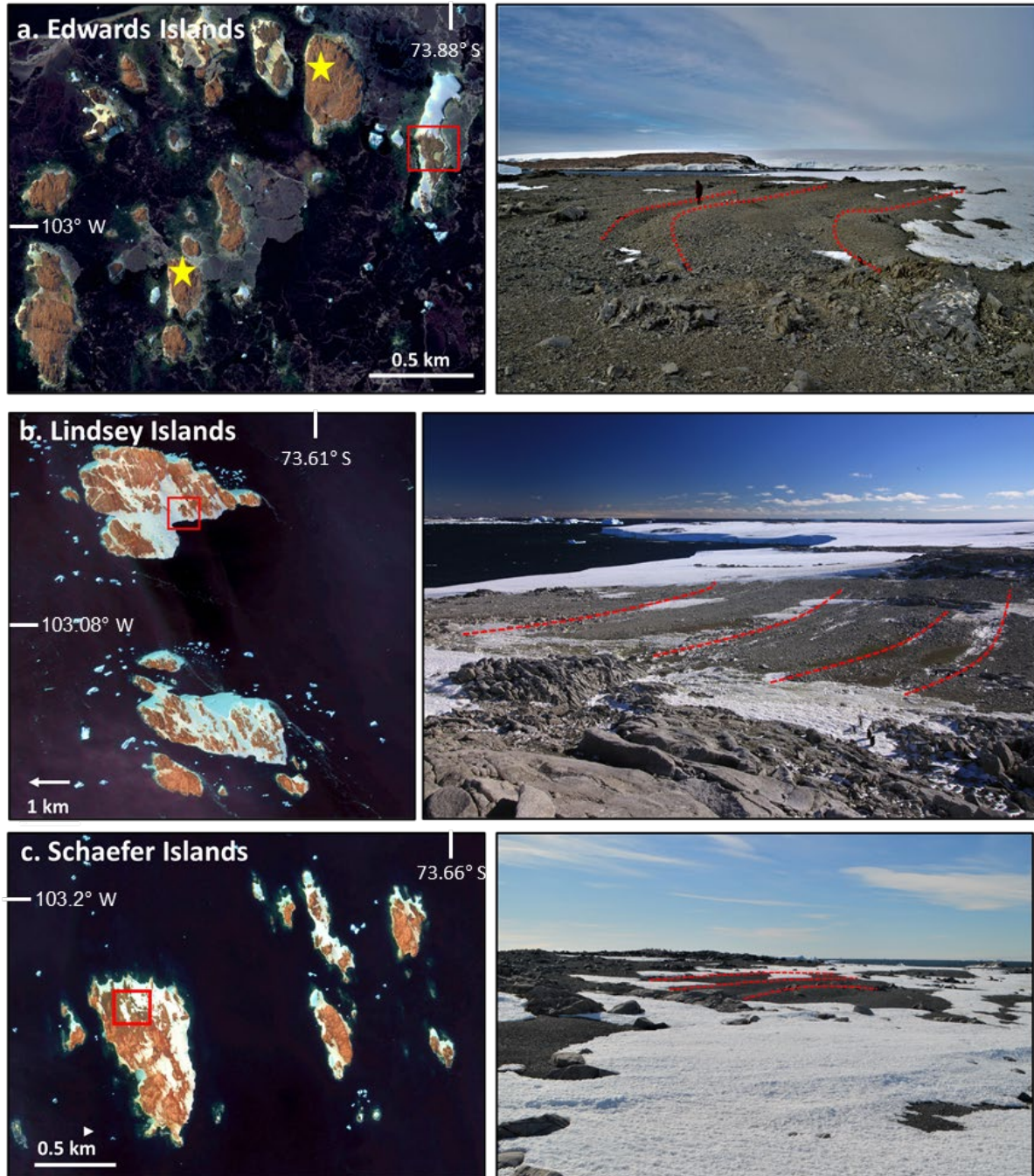
82 fall, both of which can be attributed to ice expansion when changes in global ocean
83 volumes are taken into account.

84 **Radiocarbon and Exposure-Age Results**

85 Our study focused on three largely granitic island chains (Lindsey, Schaefer, and
86 Edwards) in the Amundsen Sea Embayment (Fig. 1). Many islands display striations
87 and glacially polished bedrock at higher elevations¹⁶ (>19 meters above present-day
88 sea level [asl]). These erosional features likely restrict past sea level to <19 m elevation
89 since deglaciation, because such features are destroyed easily by wave erosion. All
90 three island chains have raised beaches (Fig. 2, Supplementary Figs. S6, S7), the
91 highest of which occur on the Lindsey Islands at ~19 m asl. Thus, available evidence
92 indicates the regional marine limit (the highest elevation reached by the post-glacial
93 sea) is at 19 m elevation. At the Schaefer and Edwards Islands, the highest discernible
94 beaches are at ~15 m and 11 m elevation, respectively, although the marine limit may
95 well be a few meters higher on the Schaefer Islands, where it was obscured by snow
96 during our visit.

97 We derived a RSL curve from 55 calibrated radiocarbon ages of shells (limpets, likely
98 *Nacella sp.*) and penguin bones (likely Adélie) extracted from raised beaches (Fig. 3a,
99 Table S1). We infer that the shells were incorporated into beaches while the mollusks
100 were still alive or shortly thereafter, so radiocarbon dates from shells date beach
101 formation and therefore contemporaneous sea level. However, it is also possible for
102 previously deposited shell to be recycled into younger beaches, so some fraction of
103 shell radiocarbon dates may represent only maximum-limiting ages for beach deposits.

104 In this study, except for three old outliers from the Schaefer Islands, shell radiocarbon
105 ages increase systematically with elevation. Furthermore, ages from similar elevations
106 are tightly clustered, and, as noted below, shell ages and a single exposure age at 8 m
107 elevation agree. Thus, we conclude that the shells afford actual – rather than apparent -
108 ages for the beaches and that the true RSL curve must pass through the shell data (Fig.
109 3a; see Supplemental Information). Extrapolating the trend in shell ages to the marine
110 limit at 19 m indicates that the marine limit dates to 5.5 ka. In contrast to the shells, we
111 infer that bone samples, mostly surface finds from relict penguin nests, were deposited
112 only after a beach uplifted above sea level. They afford minimum-limiting ages for the
113 beaches, and therefore the RSL curve must lie on or below the elevation of these
114 samples.



115

116 **Fig. 2. Satellite imagery and photographs of study sites in the Amundsen Sea**
 117 **Embayment.** Left panel shows a) Edwards Islands b) Lindsey Islands and c) Schaefer
 118 Islands from WorldView-2 imagery (copyright 2019[A], 2011[B] DigitalGlobe, Inc., a
 119 Maxar Company). Dashed lines in photos on right panels denote raised marine beaches
 120 from which shell and bone samples were collected. Photos are from sites corresponding
 121 to the red squares in adjacent imagery. Yellow stars in (a.) denote location of additional
 122 sampled islands (Photos provided in Supplementary Figs. S2,3,6).

123

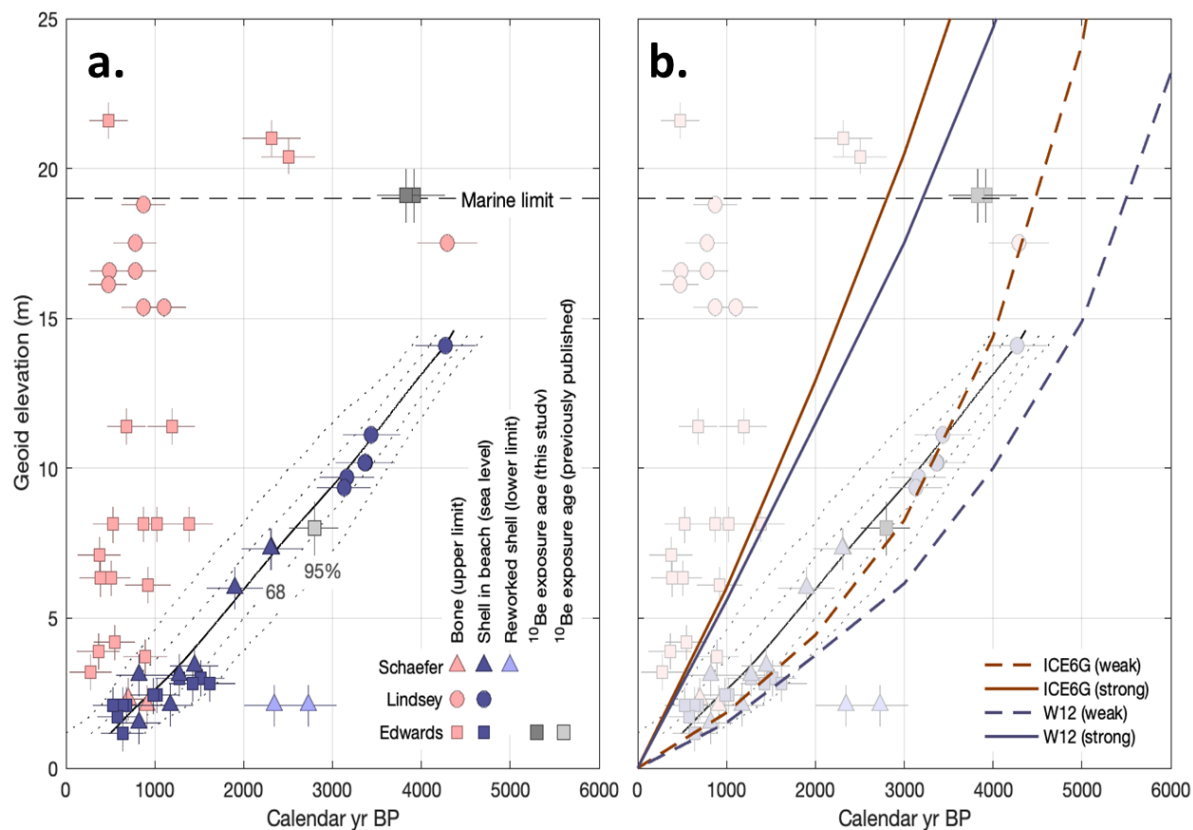
124 In addition to shells and bones, we also measured cosmogenic ^{10}Be from four bedrock
125 samples to provide additional information on the timing of deglaciation. Two samples
126 from the Lindsey Islands (LD-19-C1 and LD-19-C2), both from striated bedrock above
127 the inferred marine limit, yielded ages of 7.9 ± 0.3 ka and 8.8 ± 0.2 ka (Table S2),
128 suggesting that the islands became ice free at approximately this time. These ages are
129 younger than two published ^{10}Be bedrock exposure ages from the Lindsey Islands (See
130 SI, recalculated 10.5 ± 0.4 ka, 15.4 ± 0.7 ka¹⁶; Table S3). The latter of these was
131 excluded by Lindow et al. ¹⁶ as having prior exposure. The former also could have prior
132 exposure, but alternatively could reflect slightly earlier deglaciation of the other side of
133 the island from our samples. Our ages are the same as a similar-elevation sample from
134 the Jaynes Islands (9.0 ± 0.5 ka; ISL-3 in ¹⁶), 50 km from the Lindsey Islands.

135 In contrast to data from the Lindsey Islands, our two exposure ages from the Edwards
136 Islands yielded an average age of 3.9 ± 0.1 ka (Fig. 3a). These much-younger ages
137 may reflect either delayed deglaciation of the Edwards Islands relative to the Lindsey
138 and Schaefer Islands or emergence of the bedrock from the ocean. If the latter, the ^{10}Be
139 ages appear too young when compared to the radiocarbon-derived RSL curve.
140 Moreover, it would require the local marine limit to be at or above 19 m elevation
141 (Edwards Island samples collected at 19 m asl), something for which we did not find
142 evidence. Because of these factors, and the fact that the age of the samples is
143 approximately equal to the age of the marine limit at 11 m elevation (based on the RSL
144 curve), we favor the interpretation of delayed deglaciation, either of local glacier ice or a
145 remnant stagnant ice block, for these ages.

146 A recalculated age of 2.8 ± 0.2 ka (Fig.3a) from an erratic boulder at 8 m elevation on
147 an island 5 km north of the Edwards Islands was previously interpreted as representing
148 retreat of the Canisteo Peninsula ice front²⁶. However, this exposure age is
149 indistinguishable from radiocarbon-dated shells in beach deposits at the same
150 elevation, so must record emergence rather than deglaciation.

151 **Broader Implications of RSL Data**

152 Regardless of the interpretation of the exposure-age data, the radiocarbon-constrained
153 RSL curve (Fig. 3a) implies uninterrupted RSL fall in the Amundsen Sea Embayment
154 since 5.5 ka. We attribute this to unloading of the ice mass dominated by Thwaites and
155 Pine Island Glaciers. Although the shell data form an approximately linear array, an
156 exponential curve also could fit the data with reasonable confidence. The data indicate
157 monotonic RSL fall, which is consistent with a simple unloading history (e.g., ²⁷). More
158 complex curves, including those showing evidence of marine transgression, typically
159 reflect complicated glacial histories including re-advance (e.g. ^{23,24,28}). Our RSL curve
160 does not provide evidence for Holocene ice thickness fluctuations large enough to slow
161 or reverse isostatic rebound following early Holocene mass loss. Although we cannot
162 exclude the possibility of minor grounding-line oscillations, these RSL data do not
163 indicate significant mass fluctuations in the Amundsen Sea Embayment since 5.5 ka.



164

165 **Fig. 3. Relative sea-level reconstruction and comparison with glacial isostatic**
 166 **adjustment (GIA) models for the Amundsen Sea Embayment, Antarctica. a)** RSL
 167 curve based on radiocarbon ages of shells from raised beaches. All samples are
 168 presented as calibrated radiocarbon ages for shells and bones. The solid black line with
 169 associated bootstrap confidence intervals is an interpolation of the shell data (see
 170 supplemental information) using the method of ²⁹. The horizontal dashed black line
 171 represents the proposed regional marine limit (elevation of highest sampled beach) at
 172 19 m. Elevation errors (see methods section) associated with radiocarbon samples are
 173 represented by vertical bars on each data point and range from 0.3-0.7 m. Vertical error
 174 bars for Lindsey Island samples (0.3 m) are smaller than symbols at this scale. **b)**
 175 Comparison of RSL data with GIA model predictions derived using two different ice
 176 history models (ICE-6G_C^{30,31} and W12^{32,33}). For each ice history model, two curves are
 177 shown; these represent RSL change assuming either a strong (solid lines, upper mantle
 178 viscosity = 5×10^{20} Pa s) or a weak (dashed lines, upper mantle viscosity = 5×10^{19} Pa
 179 s) Earth model. The lithosphere thickness is set at 71 km³⁴.

180

181 Our results show that the Amundsen Sea region experienced on average ~3.5 mm/yr of
182 RSL fall between 5.5 – 0.3 ka (Fig. 3a). In contrast, bedrock uplift rates are currently 15
183 mm/yr at sites 60 - 95 km from our field sites and as much as 41 mm/yr elsewhere in
184 the Amundsen Sea Embayment²⁵. Although RSL change reflects multiple factors in
185 addition to bedrock uplift (e.g., ocean volume change), the large difference we observe
186 between modern bedrock uplift rates and Holocene RSL change requires that a recent
187 increase in the rate of viscoelastic uplift is contributing to current high rates of isostatic
188 adjustment. These rates are linked to contemporary ice-mass loss in this region²⁵, which
189 appears to be unprecedented over the last 5.5 ka.

190 The exposure ages from the Lindsey Islands, along with the radiocarbon date of 10.7 ka
191 from a reworked shell from the Schaefer Islands, indicate that the eastern Amundsen
192 Sea Embayment continental shelf was deglaciated at 11-9 ka. These ages are
193 consistent with marine geological records that show retreat of the grounding line to its
194 modern position by the early Holocene¹⁵. However, beaches apparently did not develop
195 until ~5.5 ka. Given the proximity of the islands to the current ice margin on the
196 Canisteo Peninsula (<2 km), a possible explanation for the delay is the presence of an
197 ice shelf until ~5.5 ka, as suggested by ¹⁷. An ice shelf that surrounded (but not
198 covered) the islands would prevent beaches from forming but allow marine organisms to
199 live offshore and ¹⁰Be to accumulate in exposed bedrock. This hypothesis is consistent
200 with evidence from marine sediment cores that indicate a remnant ice shelf persisted in
201 the Amundsen Sea Embayment until at least 7.5 ka³⁵. Perennial land-fast sea ice could
202 have the same effect of preventing beach formation.

203

204 **Comparison with GIA models**

205 GIA models for Antarctica typically predict RSL rise in the early Holocene, a marine limit
206 at ~ 20 m asl, and RSL fall in the mid to late Holocene^{30,33}. These GIA model results
207 agree relatively well with observations where extensive RSL data exist (e.g., the Ross
208 Sea^{27,36} and Marguerite Bay^{37,38}). Existing RSL data commonly show raised beach
209 deposits recording exponential RSL fall in the mid to late Holocene. Our RSL data from
210 Pine Island Bay display similar features. We compared our RSL data with GIA model
211 predictions generated using two different Antarctic ice-history models, ICE-6G_C^{30,31}
212 and W12^{32,33} (Fig 3b). In W12, the islands in this study become ice-free between 11-
213 10.5 ka, and in ICE6G_C, between 8.5-8.0 ka. Predictions were generated separately
214 for all three island groups but since all sites lie within 30 km, model predictions only
215 differ by ~2 m at all sites for the Late Holocene. For this reason, Fig. 3b shows the
216 averaged-RSL prediction for all three island groups. Results are shown in Fig. 3b for a
217 strong (upper mantle viscosity = 5×10^{20} Pa s) and a weak (upper mantle viscosity = $5 \times$
218 10^{19} Pa s) Earth rheology model. The Amundsen Sea Embayment is known to have a
219 relatively thin lithosphere³⁴ with a very low upper mantle viscosity²⁵. The ICE-6C_C
220 model, combined with the weaker Earth rheology model, provides the best fit to our RSL
221 data. Additionally, the exponential curve produced by the weaker Earth rheology model
222 fits within the confidence bounds of our RSL reconstruction where as that of the strong
223 Earth rheology model does not and overestimates regional Holocene RSL. However,
224 none of the models is consistent with the exposure ages on bedrock above the marine
225 limit, nor with our interpretation of the elevation of the marine limit based on the upper
226 limit of marine sediments and the lower limit of glacial polish and striations. All of the

227 GIA models in Fig. 3b predict that the exposure-age samples at 19 - 26 m elevation
228 should have been under water at the time of deglaciation and consequently not exposed
229 to cosmic radiation. Therefore, although the ICE-6G_C (weak) model fits our RSL data
230 between 0 - 4 ka (Fig. 3b), we infer that none of the models considered here accurately
231 captures the mid to late Holocene RSL history of the region.

232 In summary, the Holocene RSL record presented here puts into context the current
233 rapid bedrock uplift near the grounding lines of Thwaites and Pine Island glaciers and
234 shows a monotonic fall in RSL since the mid-Holocene. Although the resolution of the
235 RSL curve does not preclude the possibility of minor marginal fluctuations of Thwaites
236 and Pine Island glaciers during the past ~ 5.5 ka, this record is best explained by the
237 hypothesis that ice reached close to its current margin in the mid-Holocene and has
238 remained in the vicinity of that position since, without large-scale glacier recession or re-
239 advance. Thus, there remains no direct evidence that Thwaites and Pine Island Glaciers
240 were smaller than present during the present interglacial period, and the present-day
241 rate of ice recession appears to be unprecedented in the last ~5.5 ka.

242

243 **Methods**

244 *Field sampling*

245 Field operations were part of cruise NBP1902 conducted from the U.S. research vessel,
246 the Nathaniel B. Palmer. Marine organic material (shells, likely from the limpet *Nacella*,
247 and bones – likely from Adelie penguins [Fig S7]) were collected from raised marine
248 beaches. Samples were found beneath boulders (up to 25 cm diameter) or in ~0.5 m

249 deep excavations. We collected a minimum of three samples from each beach where
250 possible. We avoided surface samples, because they are more likely to be modern in an
251 area heavily colonized by penguins at the present day. Samples for exposure-age
252 dating were collected from bedrock outcrops using a hammer and chisel. There was no
253 topographic shielding.

254
255 We determined the elevation relative to sea level (here defined as the EGM96 geoid) of
256 at least one location on each distinct raised beach using a Septentrio APS3 high-
257 precision GPS unit with differential correction relative to a temporary base station
258 deployed during each sampling period and located additional sample locations using
259 uncorrected handheld GPS. To determine the elevation of sample locations lacking
260 DGPS positions, but that are still located on corresponding beach ridges, we used
261 photogrammetric digital elevation models (DEMs) of each island group prepared by the
262 Polar Geospatial Center from DigitalGlobe satellite imagery. We registered each DEM
263 to the DGPS data by applying a vertical offset determined to minimize mean square
264 differences between DEM and DGPS elevations for DGPS survey points, and then
265 sampled elevations from the corrected DEMs for all sample locations. The elevation
266 uncertainty is estimated from the distribution of the residuals between the DGPS points
267 and the elevations of the corrected DEMs at those locations, and ranges from 0.3-0.7
268 m. We applied the DEM-derived elevation uncertainties to all samples in Fig. 3 to
269 account for undulations in beach ridges.

270

271

272 *Radiocarbon dates*

273 Radiocarbon samples were prepared at the University of Maine Glacial Geology and
274 Geochronology Laboratory, USA. We cleaned shell samples in ultrapure water
275 overnight in an ultrasonic bath before drying, weighing, and shipping them to the
276 National Ocean Sciences Accelerator Mass Spectrometry (NOSAMS) facility for dating.
277 For bone samples, we extracted collagen following procedures modified from the
278 University of California - Santa Cruz Stable Isotope Laboratory
279 (https://websites.pmc.ucsc.edu/~silab/ea.collagen_SOP.php). Pieces (50-100 mg) of
280 bone were washed in ultrapure water for 24 hours in a sonicator and dried overnight.
281 Then, samples were decalcified in a 0.5N HCL solution for 24 – 48 hours. Next, we
282 rinsed the samples and let them sit in ~10 ml of 0.1N NaOH solution overnight to
283 remove contaminants. To defat samples, they were subjected to multiple baths in
284 petroleum ether while in an ultrasonic bath. Last, we rinsed and dried the collagen
285 samples before sending them to the Environmental Geochemistry Laboratory at Bates
286 College in Lewiston, Maine, for carbon/nitrogen ratio (C:N) analysis. Samples with a
287 C:N ratio between 2.9 to 3.6 were considered to have sufficiently well-purified collagen
288 to be suitable for radiocarbon dating³⁹. We sent collagen samples within the appropriate
289 C:N range to the NOSAMS facility for radiocarbon dating. Resultant radiocarbon ages
290 were converted to cal. yr BP using CALIB version 8.1⁴⁰ and the Marine20 calibration
291 dataset⁴⁰. Although this calibration dataset is not optimized for polar regions⁴¹, it is the
292 best correction available at present (P. Reimer, personal communication, 2021). We
293 applied a delta-R value of 610 ± 110 yr, recalculated from the Holocene Antarctic coral
294 dataset⁴² for specific use with Marine2020.
295

296 *Cosmogenic exposure age dating*

297 Four bedrock samples were processed at the University of Maine Cosmogenic Isotope
298 Laboratory. We crushed and sieved samples and subjected them to froth flotation,
299 followed by a sequence of HF:HNO₃ leaches to isolate pure quartz (as determined by
300 ICP-OES). We weighed approximately 30 g of pure quartz for each sample and spiked
301 them with an in-house ¹⁰Be carrier made from phenakite. Following standard ion-
302 exchange chemistry⁴³, samples were precipitated as hydroxides, converted to BeO, and
303 then packed in cathodes with niobium. ¹⁰Be/⁹Be ratios were measured at the Center for
304 Accelerator Mass Spectrometry at Lawrence Livermore National Laboratory, USA.
305 Samples ran with high ⁹Be currents (20-30 microamps). The full ¹⁰Be/⁹Be procedural
306 blank for the batch was 3.6E⁻¹⁶. We calculated ages with version 3 of the online
307 exposure age calculator described by ⁴⁴ and subsequently updated using the default
308 calibration data set⁴⁵ and “St” scaling^{46,47}. Ages in the text are given with 1-sigma
309 internal errors, whereas those plotted on the RSL curve are shown with 1-sigma
310 external errors that incorporate uncertainties in production rate and scaling for more
311 realistic comparison to radiocarbon ages.

312 **References**

- 313 1. Bamber, J. L., Oppenheimer, M., Kopp, R. E., Aspinall, W. P., Cooke, R. M. Ice
314 sheet contributions to future sea-level rise from structured expert judgment.
315 *Proceedings of the National Academy of Sciences*, **116(23)**, 1195–1120 (2019).
- 316 2. Rignot, E. et al. Four decades of Antarctic Ice Sheet mass balance from 1979-
317 2017. *Proceedings of the National Academy of Sciences* **116(4)**, 1095 – 1103
318 (2019).
- 319 3. Milillo, P. et al. Heterogeneous retreat and ice melt of Thwaites Glacier, West
320 Antarctica. *Science Advances*, **5(1)**, eaau3433 (2019).
321
322

- 323 4. Pritchard, H. et al. Antarctic ice-sheet loss driven by basal melting of ice shelves.
324 *Nature* **484**, 502-505 (2012).
325
- 326 5. Holland, D., Nicholls, K., Basinski, A. The Southern Ocean and its interaction
327 with the Antarctic Ice Sheet. *Science* **367** 1326-1330 (2020).
328
- 329 6. Joughin, I., and Alley, B. R. Stability of the West Antarctic ice sheet in a warming
330 world. *Nature Geoscience* **4**, 506-513 (2011)
331
- 332 7. Rignot, E., Mouginot, J., Morlighem, M., Seroussi, H., & Scheuchl, B.
333 Widespread, rapid grounding line retreat of Pine Island, Thwaites, Smith, and
334 Kohler glaciers, West Antarctica, from 1992 to 2011. *Geophysical Research*
335 *Letters* **41(10)**, 3502–3509 (2014)
- 336
- 337 8. Hughes, T., 1981. The Weak Underbelly of the West Antarctic Ice-Sheet. *Journal*
338 *of Glaciology* **27**, 518-525 (1981).
339
- 340 9. DeConto, R. M., & Pollard, D. (2016). Contribution of Antarctica to past and
341 future sea-level rise. *Nature* **531**, 591–597 (2016).
- 342 10. Fretwell, H.D. et al. Bedmap2: improved ice bed, surface and thickness datasets
343 for Antarctica. *Cryosphere* **7**, 375-393 (2013).
344
- 345 11. Hogan, K. A. et al. Revealing the former bed of Thwaites Glacier using sea-floor
346 bathymetry. *The Cryosphere* **14**, 2883-2908 (2020)
347
- 348 12. Nitsche, F. et al. Paleo ice flow and subglacial meltwater dynamics in Pine Island
349 Bay, West Antarctica. *The Cryosphere* **7**, 249–262 (2013).
350
- 351 13. Graham, A.G.C. et al. Flow and retreat of the Late Quaternary Pine Island-
352 Thwaites palaeo-ice stream, West Antarctica. *J. Geophys. Res* **115**, F03025
353 (2010).
354
- 355 14. Larter, R.D. et al. Reconstruction of changes in the Amundsen Sea and
356 Bellingshausen Sea sector of the West Antarctic Ice Sheet since the Last Glacial
357 Maximum. *Quaternary Science Reviews* **100**, 55–86 (2014).
358
- 359 15. Hillenbrand, C. -D. et al. Grounding-line retreat of the West Antarctic Ice Sheet
360 from inner Pine Island Bay. *Geology* **41**, 35-38 (2013).
361
- 362 16. Lindow, J. et al. Glacial retreat in the Amundsen Sea sector, West Antarctica –
363 first cosmogenic evidence from central Pine Island Bay and the Kohler Range.
364 *Quaternary Science Reviews*. **98**, 166–173 (2014).
365

- 366 17. Johnson, J.S. et al. Rapid thinning of Pine Island Glacier in the early Holocene.
367 *Science* **343**, 999–1001 (2014).
368
- 369 18. Johnson, J.S. et al. Deglaciation of Pope Glacier implies widespread early
370 Holocene ice sheet thinning in the Amundsen Sea sector of Antarctica. *Earth and*
371 *Planetary Science Letters* **548**, 116501 (2020).
372
- 373 19. Joughin, I., Smith, B., Medley, B. Marine Ice Sheet Collapse Potentially Under
374 Way for the Thwaites Glacier Basin, West Antarctica. *Science* **344**, 735-738
375 (2014).
376
- 377 20. DeConto, R. M., & Pollard, D. (2016). Contribution of Antarctica to past and
378 future sea-level rise. *Nature* 531, 591–597 (2016).
379
- 380 21. Howat, I. M., Porter, C., Smith, B. E., Noh, M.-J., and Morin, P. The Reference
381 Elevation Model of Antarctica. *The Cryosphere* **13**, 665-674 (2019).
382
- 383 22. Weatherall P. et al. The GEBCO_2019 Grid - a continuous terrain model of the
384 global oceans and land. British Oceanographic Data Centre, National
385 Oceanography Centre, NERC, UK. doi:10/c33m (2019).
386
- 387 23. Motyka, R. Little Ice Age subsidence and post Little Ice Age uplift at Juneau,
388 Alaska, inferred from dendrochronology and geomorphology. *Quaternary*
389 *Research* **59**, 300-309 (2003).
390
- 391 24. Hall, B. L. Holocene relative sea-level changes and ice fluctuations in the South
392 Shetland Islands. *Global and Planetary Change* **74(1)**, 15–26 (2010).
393
- 394 25. Barletta, V. et al. Observed rapid bedrock uplift in Amundsen Sea Embayment
395 promotes ice-sheet stability. *Science* **360**, 1335-1339 (2018).
396
- 397 26. Johnson, J.S., Bentley, M.J., Gohl, K. First exposure ages from the Amundsen
398 Sea Embayment, West Antarctica: the Late Quaternary context for recent
399 thinning of Pine Island, Smith, and Pope Glaciers. *Geology* **36**, 223–226 (2008).
400
- 401 27. Hall, B., Baroni, C., Denton, G. Holocene relative sea-level history of the
402 Southern Victoria Land Coast, Antarctica. *Global and Planetary Change* **42**, 241-
403 263 (2004).
404
- 405 28. Simms, A.R., Ivins, E.R., DeWitt, R., Kouremenos, P., Simkins, L.M. Timing of
406 the most recent Neoglacial advance and retreat in the south Shetland Islands,

- 407 Antarctic Peninsula: insights from raised beaches and Holocene uplift rates.
408 *Quaternary Science Reviews* **47**, 41-55 (2012).
409
- 410 29. Lougheed, B. C., & Obrochta, S. P. A Rapid, Deterministic Age-Depth Modeling
411 Routine for Geological Sequences With Inherent Depth Uncertainty.
412 *Paleoceanography and Paleoclimatology* **34**, 122–133 (2019).
- 413 30. Argus, D. F., Peltier W. R., Drummond, R., Moore. A. W. The Antarctic
414 component of post glacial rebound Model ICE-6G_C (VM5a) based upon GPS
415 positioning, exposure age dating of ice thicknesses and sea level histories,
416 *Geophysical Journal International* **198**, 537–563 (2014).
417
- 418 31. Peltier, W. R., Argus, D. F., Drummond, R. Space geodesy constrains ice age
419 terminal deglaciation: The global ICE-6G_C (VM5a) model. *Journal of*
420 *Geophysical Research: Solid Earth* **120**, 450–487 (2015).
421
- 422 32. Whitehouse, P. L., Bentley, M. J., Le Brocq, A. M. A deglacial model for
423 Antarctica: Geological constraints and glaciological modeling as a basis for a
424 new model of Antarctica glacial isostatic adjustment. *Quaternary Science*
425 *Reviews* **32**, 1–24 (2012a).
426
- 427 33. Whitehouse, P. L., Bentley, K. J., Milne, G. A., King, M., Thomas, I. D. A new
428 glacial isostatic adjustment model for Antarctica: Calibrated and tested using
429 observations of relative sea level change and present day uplift rates.
430 *Geophysical Journal International* **190**, 1464–1482 (2012b).
431
- 432 34. Heeszel, D. S. et al. Upper mantle structure of central and West Antarctica from
433 array analysis of Rayleigh wave phase velocities. *Journal of Geophysical*
434 *Research: Solid Earth* **121**, 1758–1775 (2016).
435
- 436 35. Hillenbrand, C.-D. et al. West Antarctic Ice Sheet retreat driven by Holocene
437 warm water incursions. *Nature* **547**, 43–48 (2017).
438
- 439 36. Baroni, C., and Hall, L. H. A new Holocene relative sea-level curve for Terra
440 Nova Bay, Victoria Land, Antarctica. *Journal of Quaternary Science* **19**, 377-396
441 (2004).
442
- 443 37. Bentley, M., Hodgson, D., Smith, J., & Cox, N. Relative sea level curves for the
444 South Shetland Islands and Marguerite Bay, Antarctic Peninsula. *Quaternary*
445 *Science Reviews* **24**, 1203–1216 (2005).
446
- 447 38. Simkins, L. M., Simms, A. R., & DeWitt, R. Relative sea-level history of
448 Marguerite Bay, Antarctic Peninsula derived from optically stimulated
449 luminescence-dated beach cobbles. *Quaternary Science Reviews* **77**, 141–155
450 (2013).
451

- 452 39. Ambrose, S.H. Preparation and Characterization of Bone and Tooth Collagen for
453 Isotopic Analysis. *Journal of Archaeological Science* **17**, 431-451 (1990).
454
- 455 40. Stuiver, M., Reimer, P.J., Reimer, R.W., 2021, CALIB 8.2 [WWW program] at
456 <http://calib.org>, accessed 2021-3-30
457
- 458 41. Heaton, T., et al. Marine20—The Marine Radiocarbon Age Calibration Curve (0–
459 55,000 cal BP). *Radiocarbon*, **62**, 779-820 (2020).
460
- 461 42. Hall, B. L., Henderson, G. M., Baroni, C., & Kellogg, T. B. Constant Holocene
462 Southern-Ocean ¹⁴C reservoir ages and ice-shelf flow rates. *Earth and Planetary
463 Science Letters* **296**, 115–123 (2010).
464
- 465 43. Hall, B. L., Lowell, T. V., & Brickle, P. Multiple glacial maxima of similar extent at
466 ~20–45 ka on Mt. Osborne, East Falkland, South Atlantic region. *Quaternary
467 Science Reviews* **250**, 106677 (2020).
468
- 469 44. Balco, G., Stone, J., Lifton, N., Dunai, T. A complete and easily accessible
470 means of calculating surface exposure ages or erosion rates from ¹⁰Be and ²⁶Al
471 measurements. *Quaternary Geochronology* **3**, 174-195 (2008).
472
- 473 45. Borchers B. et al. Geological calibration of spallation production rates in the
474 CRONUS-Earth project. *Quaternary Geochronology* **31**, 188–198 (2016).
475
- 476 46. Lal, D. Cosmic ray labeling of erosion surfaces: in situ nuclide production rates
477 and erosion models. *Earth and Planetary Science Letters* **104**, 424 – 439 (1991).
478
- 479 47. Stone, J. O. Air pressure and cosmogenic isotope production. *Journal of
480 Geophysical Research* **105**, 23,753 – 23,759 (2000).
481

482

483 **Corresponding Author**

484 For correspondence and requests for materials, please contact Brenda Hall
485 (brendah@maine.edu) or Scott Braddock (scott.braddock@maine.edu).
486

487 **Acknowledgements**

488 This work is part of the “Geological History Constraints” project, a component of the
489 International Thwaites Glacier Collaboration. We thank C. Beeler, N. Fenney, V.

490 Fitzgerald, A. Fox, K. Hogan, J. Kirkham, E. Rush, UNAVCO, the Polar Geospatial
491 Center, and the Captain and Crew of the R/V Nathaniel B. Palmer for assistance. This
492 work was supported by the National Science Foundation (Grant OPP-1738989 – SB,
493 BH, GB, MS, BG, SC) and the Natural Environment Research Council (Grant
494 NE/S006710/1 and NE/S006753/1 – JJ, DR, JW). This is ITGC Contribution No. ITGC-
495 050.

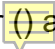
496
497 **Author Contributions**

498 G. B., S. C., B. G., B. H., J. J., D. R., and J. W. conceived the overarching “Geological
499 History Constraints” project of the International Thwaites Glacier Collaboration. B. H.
500 developed and directed the RSL component. S. B. and M. S. carried out the fieldwork
501 and collected the samples. S. B. and B. H. performed laboratory work. P. W. provided
502 GIA model output. G. B. constructed the age model for the RSL curve. S. B. and B. H.
503 wrote the paper with contributions from all authors.

504
505 **Competing Interests Statement**

506 The authors declare no competing interests.

507
508 **Data Availability**

509 The authors state that all data supporting the findings of this study are available in the
510 paper and in the Supplementary Information. They also can be found in public
511 databases, including the the United States Antarctic Program Data Center  and the
512 ICE-D cosmogenic database (<https://version2.ice-d.org/antarctica/site/EDWARDSIS/> and
513 <https://version2.ice-d.org/antarctica/site/LINDSI/>).

